Anisotropy and magnetotransport in ordered magnetic antidot arrays

F. J. Castaño, K. Nielsch, C. A. Ross,[a] J. W. A. Robinson, and R. Krishnan
Department of Materials Science and Engineering, Massachusetts Institute of Technology, Cambridge, Massachusetts 02139

(Received 16 April 2004; accepted 3 August 2004)

Magnetic films containing ordered arrays of holes ("antidots") with period ~200 nm have been prepared using porous anodic alumina substrates with square and hexagonal symmetries. Large area (~cm^2) single-layer CoFe ordered antidot arrays show well-defined in-plane magnetic anisotropy related to the symmetry of the arrays, and the anisotropic magnetoresistance is smaller than that of a continuous film. For NiFe/Cu/CoFe antidot arrays, the giant magnetoresistance ratio of the patterned films is of similar magnitude to that of the unpatterned film, and shares the symmetry of the substrate. This behavior is attributed to the geometry of the antidots, which confine the magnetization of each layer parallel to the current flow. © *2004 American Institute of Physics*. [DOI: 10.1063/1.1800281]

Magnetic films containing holes or "antidots" have properties very different from those of unperforated films. The holes introduce shape anisotropies which allow the nucleation and movement of domain walls, the net in-plane anisotropy, and associated properties such as magnetoresistance to be controlled. Measurements on these structures enable insight to be gained into the magnetic behavior of confined geometries, which is complementary to the extensive literature on magnetic particles. The majority of work on antidot arrays has been carried out on films with square, rectangular, or circular holes with dimensions and spacings on the micron or half micron scale.[1–9] On these length scales, magnetic imaging shows that well-defined domain structures exist. The shape anisotropy of the holes leads to complex remanent states including periodic domain structures that depend on the direction of the magnetic field and the intrinsic anisotropy axis. The regions between the holes, perpendicular to the magnetization direction, have even been proposed as data storage domains.[1–3] Reversal occurs by the passage of domain walls through the structure, and pinning at the antidots leads to an enhanced coercivity compared to the unpatterned film. Micromagnetic modeling[8–10] confirms the presence of domain walls and regions with different magnetization directions, due to the tendency of the magnetization to follow the edges of the antidots.

There is relatively little published data on antidot arrays with deep submicron periodicity, although the domain morphology differs considerably from that of larger period arrays.[6,7,11,12] Experimentally, in this size regime the fabrication of regular arrays of antidots requires the use of electron beam or focused ion beam lithography, which limits the area of sample that can be made. To create larger area samples suitable for conventional magnetometry, films can be deposited over self-assembled porous templates, such as anodic alumina films, to form a porous metal film.[13–15] Porous alumina films with greatly improved pore size control and short-range order can be made using a two-step anodization process,[16,17] and Ni films grown onto such substrates, with 40–70 nm antidot diameters, show higher magnetoresistance, coercivity, and remanence than continuous films.[14] However, in these antidot arrays it is not possible to quantify the in-plane anisotropy resulting from the symmetry of the array because the two-dimensional pore array lacks long-range order over distances greater than about ten times the pore period. Additionally, although anisotropic magnetoresistance has been reported for small period antidot arrays,[15] there have been no reports on giant magnetoresistive multilayer antidot arrays. We report here a study of the in-plane anisotropy, coercivity, and magnetoresistance of CoFe single layer and NiFe/Cu/CoFe pseudo-spin-valve (PSV) antidot arrays deposited on top of anodic alumina templates with ~200 nm periods and square or hexagonal symmetries. The antidot arrays investigated here differ from previous work in having long-range order over several square cm, allowing a study to be made of the effect of array geometry on the in-plane anisotropy of the hysteresis and magnetoresistance.

To prepare the samples, 10-cm-diam thermally oxidized (100) silicon wafers were coated with a trilayer resist stack[18] and the top resist layer was patterned with a grid of holes by two consecutive interference lithography exposures.[19] Both hexagonal hole patterns with a periodicity of 208 nm and square hole patterns with a periodicity of 180 nm were made. These hole patterns were transferred from the resist into the 40-nm-thick oxide layer using reactive ion etching, then into the silicon substrate using an anisotropic KOH etch (20 wt%, 5 min), to create an array of inverted pyramids [Figs. 1(a) and 1(b)]. A 300-nm-thick aluminum film was deposited conformally over the inverted pyramid arrays and anodized in phosphoric acid (5 wt%) at 3 °C and 80–82 V. This creates an anodic alumina film containing parallel vertical pores. The pores form preferentially at the dimples in the aluminum film, directly above the vertices of the inverted pyramids. Since the inverted pyramids are slightly rectangular, there can be a placement uncertainty of up to ~20 nm in the pore positions. Magnetic CoFe(10 nm) films and CoFe(5.5 nm)/Cu (3 or 6 nm)/NiFe (6 nm) multilayers were then dc-triode-sputtered from 3-in.-diam $Co_{84}Fe_{16}$, $Ni_{80}Fe_{20}$ and Cu targets onto the porous alumina templates and also onto smooth thermally oxidized (100) wafers. The base pressure was below 5×10^{-9} Torr and the argon pressure during growth was 1 mTorr. All samples were capped with 3 nm Cu to prevent oxidation. The sputter guns produce an

[a]Electronic mail: caross@mit.edu

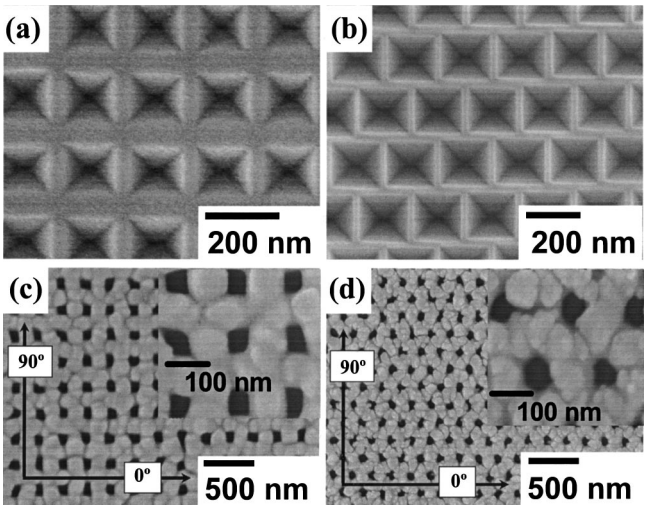

FIG. 1. Scanning electron micrographs of the inverted pyramid square (a) and hexagonal (b) templates etched into Si(100), and the square (c) and hexagonal (d) CoFe magnetic antidot arrays with 70-nm-square pores and 80-nm-diameter pores, respectively. The insets show higher magnification images.

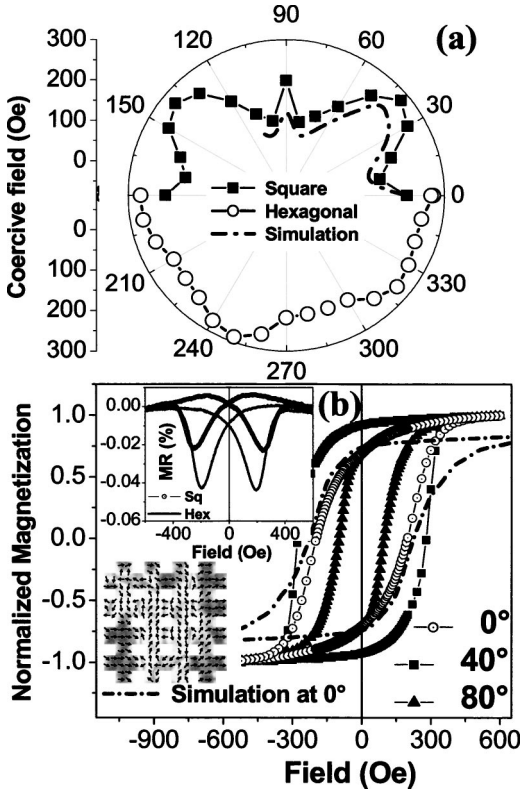

FIG. 2. (a) Angular dependence of the coercivity of the CoFe square and hexagonal antidot structures, and the results of the micromagnetic model for the square structure. (b) Hysteresis loops from the square CoFe antidot array for selected applied field directions. The dashed line shows a simulated hysteresis loop for an applied field along the 0° direction. The upper inset shows magnetoresistance curves of the square and hexagonal CoFe antidot arrays, for a magnetic field along the 0° direction. The simulated magnetic configuration at an applied field of 300 Oe is depicted in the lower inset.

in-plane magnetic field of 20 Oe during film growth and the templates were aligned so that this field coincided with the 0° direction [see Figs. 1(c) and 1(d)]. This *in situ* field introduces a weak in-plane uniaxial anisotropy in magnetic films on smooth substrates. Hysteresis loops were measured on 5 $\times 10$ mm^2 samples using an alternating gradient magnetometer and a vibrating sample magnetometer, and magnetoresistance was measured using the four-point probe technique with contacts arranged linearly and the applied field always parallel to the current. The sense current was 20 mA and the arrays were measured at 10° increments from the 0° direction to map the in-plane anisotropy.

The coercivity, hysteresis loops, and magnetoresistance curves of single layer 10-nm-thick CoFe antidot arrays are depicted in Fig. 2. The square and hexagonal templates induce well-defined fourfold and sixfold anisotropies which completely mask the growth-induced anisotropy. The slight distortions from perfect fourfold or sixfold symmetries are most likely due to a slight rectangular distortion of the arrays. The coercivity is largest, ~200 Oe, when applying a magnetic field along the closest-packed directions of the arrays. On the other hand, the remanence is highest along the magnetically harder directions (40° and 60° for the square and hexagonal arrays, respectively) and is almost constant for the other applied field directions.

The behavior of the square CoFe array was compared with a micromagnetic simulation, performed using two-dimensional OOMMF software from NIST on a 5×5 square-hole array with dimensions identical to those in Fig. 1(c). The structure was discretized into 5 nm $\times$ 5 nm square elements and hysteresis loops were calculated using parameters for bulk cubic CoFe alloys with random magnetocrystalline anisotropy. Figure 2(b) shows both the hysteresis loop and a snapshot of the domain structure at a magnetic field of −300 Oe after positive saturation along the 0° direction. At remanence after saturation, the magnetization is aligned along the continuous strips of magnetic material that lie parallel to the original applied field. However, in the regions between the antidots, the magnetization tilts in plane to remain parallel to the edges of the antidots,[20] so that the moment does not saturate until >2 kOe. The structure is magnetically softer if the field is applied a few degrees away from the 0° and 90° directions, while along the 45° degree direction the coercivity is greatest. Our OOMMF modeling predicts in-plane anisotropy in the coercivity which is in excellent agreement with experimental data [see Fig. 2(a)], although it predicts a slower approach to saturation than is observed experimentally.

The anisotropic magnetoresistance ratio (AMR) for both square and hexagonal CoFe antidot arrays shows two distinct minima [see inset in Fig. 2(b)], which correlate with the switching field of the arrays. The AMR is 0.25% for the CoFe film and significantly lower for the antidot structures (0.04% and 0.02% for the square and hexagonal arrays, respectively). Transport modeling of 20-nm-thick NiFe antidot square arrays with similar lateral dimensions to those of our samples[20] shows that the majority of the current flows along the strips of the film that are parallel to the current flow (and to the applied field), with a much lower current density in the material that lies between the antidots. For a 200 nm period structure with 100-nm-diam antidots, this model predicts that the antidot array has an AMR that is 20 times smaller than the unpatterned NiFe, in good agreement with our data. This reduction in AMR can be attributed to the fact that the magnetization in the continuous horizontal strips of the array, where most of the current flows, is constrained to lie parallel or antiparallel to the current, and from the occurrence of electron scattering from the antidot edges.

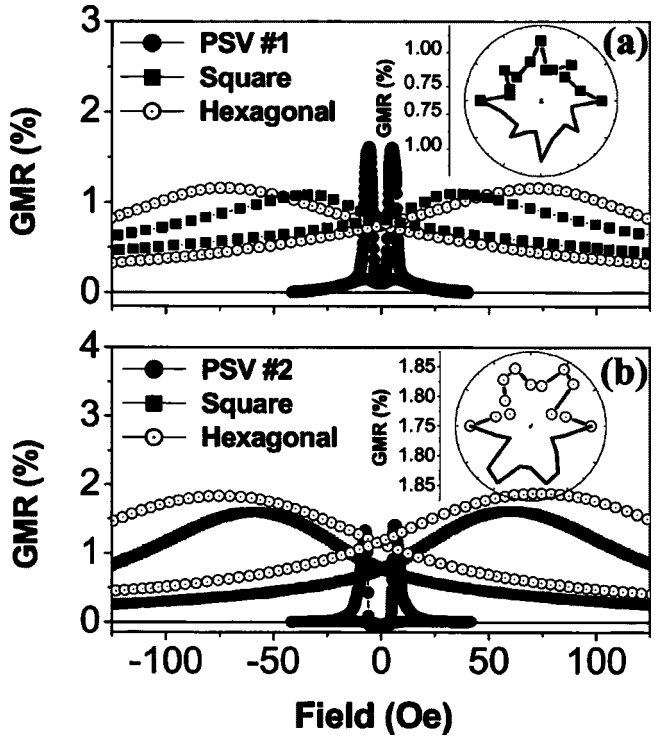

FIG. 3. Giant magnetoresistance data for (a) NiFe(6 nm)/Cu(3 nm)/CoFe(5.5 nm) (PSV1) and (b) NiFe(6 nm)/Cu(6 nm)/CoFe(5.5 nm) (PSV2) thin film structures. The inset to (a) shows the angular distribution for the GMR of the square array of PSV1, while the inset to (b) shows the GMR of the hexagonal array of PSV2. The field was applied along the 0° direction.

The behavior of the giant magnetoresistance (GMR) ratio in the PSV antidot arrays is of particular interest. GMR curves for patterned and unpatterned PSV 1 (3 nm Cu spacer) and PSV2 (6 nm Cu spacer) films are shown in Fig. 3. As expected, the GMR data correlate with the magnetic hysteresis loops (not shown). In the unpatterned PSVs, the NiFe (soft) and CoFe (hard) layers reverse abruptly at fields of a few Oe giving a sharply varying GMR response as a function of applied field. The GMR ratios for PSV1 and PSV2 unpatterned films are 1.6% and 1.4% respectively. In the antidot arrays the hysteresis loop is considerably broadened, similar to the data in Fig. 2(b), and the two-step reversal is evident as a change in slope of the loop. For the square and hexagonal antidot arrays the GMR is maximum at fields of 30 and 75 Oe for PSV1 and 60 and 80 Oe for PSV2, and the magnitude of the GMR is similar to that of the unpatterned films. The thinner Cu results in a lower switching field and higher GMR. The GMR follows the symmetry of the antidot arrays [see insets in Figs. 3(a) and 3(b)]. Scattering from the edges of the antidots, plus the roughness of the film that is evident from Fig. 1, are expected to reduce the GMR compared to the unpatterned film, so the high GMR measured for the antidot arrays is attributed to the predominantly parallel or antiparallel alignment of the magnetization in the CoFe and NiFe layers within the strips of film parallel to the field and the current. This occurs because the magnetization follows the edges of the antidots.

In conclusion, we have fabricated long-range ordered single-layer and PSV antidot arrays with periods of approximately 200 nm using porous alumina substrates with square and hexagonal symmetries. Single layer CoFe antidot arrays show in-plane magnetic anisotropy which follows the symmetry of the array, hysteresis behavior in agreement with a micromagnetic model, and AMR smaller than the unpatterned film. However, CoFe/Cu/NiFe multilayer films show a high GMR because the magnetization directions of the two magnetic layers are constrained by the shape anisotropy of the array. The use of large area porous alumina substrates, with geometries controlled by templating the pore formation, allows the symmetry, magnetic hysteresis properties, and magnetoresistance of thin films to be controlled.

This work was supported by the National Science Foundation under Grant No. 0210321. The authors thank Henry I. Smith for use of nanofabrication facilities.

[1] R. P. Cowburn, A. O. Adeyeye, and J. A. C. Bland, Appl. Phys. Lett. **70**, 2309 (1997).
[2] R. P. Cowburn, A. O. Adeyeye, and J. A. C. Bland, J. Magn. Magn. Mater. **173**, 193 (1997).
[3] A. O. Adeyeye, J. A. C. Bland, and C. Daboo, Appl. Phys. Lett. **70**, 3164 (1997).
[4] Y. Otani, S. G. Kim, T. Kohda, and K. Fukamichi, IEEE Trans. Magn. **34**, 1090 (1998).
[5] D. R. Lee, Y. Choi, C. Y. Youm, J. C. Lang, D. Haskel, G. Srajer, V. Metlushko, B. Ilic, and S. D. Bader, Appl. Phys. Lett. **81**, 4997 (2002).
[6] L. J. Heyderman, F. Nolting, and C. Quitmann, Appl. Phys. Lett. **83**, 1797 (2003).
[7] L. J. Heyderman, H. H. Solak, F. Nolting, and C. J. Quitmann, J. Appl. Phys. **95**, 6651 (2004).
[8] C. Yu, M. J. Pechan, and G. J. Mankey, Appl. Phys. Lett. **83**, 3948 (2003).
[9] L. Torres, L. Lopez-Diaz, and J. Iniguez, Appl. Phys. Lett. **73**, 3766 (1998).
[10] C. T. Yu, H. Jiang, L. Shen, P. J. Flanders, and G. J. Mankey, J. Appl. Phys. **87**, 6322 (2000).
[11] M. B. A. Jalil, J. Appl. Phys. **93**, 7053 (2003).
[12] I. Guedes, N. J. Zaluzec, M. Grimsdich, V. Metlushko, P. Vavassori, B. Ilic, P. Neuzil, and R. Kumar, Phys. Rev. B **62**, 11719 (2000).
[13] J. A. Barnard, A. Butera, H. Fujiwara, V. R. Inturi, J. D. Jarratt, T. J. Klemmer, T. W. Scharr, and J. L. Weston, J. Appl. Phys. **81**, 5467 (1997).
[14] K. Liu, S. M. Baker, M. Tuominen, T. P. Russell, and I. K. Schuller, Phys. Rev. B **63**, 060403 (2001).
[15] Z. L. Xiao, C. Y. Han, U. Welp, H. H. Wang, V. K. Vlasko-Vlasov, W. K. Kwok, D. J. Miller, J. M. Hiller, R. E. Cook, G. A. Willing, and G. W. Crabtree, Appl. Phys. Lett. **81**, 2869 (2002).
[16] H. Masuda and K. Fukuda, Science **268**, 1466 (1995).
[17] H. Masuda, H. Asoh, M. Watanabe, M. K. Nishio, M. Nakao, and T. Tamamura, Adv. Mater. (Weinheim, Ger.) **13**, 189 (2001).
[18] M. L. Schattenburg, R. J. Aucoin, and R. C. Fleming, J. Vac. Sci. Technol. B **13**, 3007 (1995).
[19] C. A. Ross, S. Haratani, F. J. Castaño, Y. Hao, M. Hwang, M. Shima, J. Y. Cheng, B. Vogeli, M. Farhoud, M. Walsh, and H. I. Smith, J. Appl. Phys. **91**, 6848 (2002).
[20] J. Guo and M. B. A. Jalil, J. Appl. Phys. **93**, 7450 (2003).